Research Article

Qiuju Chen, Tao Hui, Hongjuan Sun, Tongjiang Peng, Wenjin Ding*

Synthesis of magnesium carbonate hydrate from natural talc

https://doi.org/10.1515/chem-2020-0154
received February 01, 2020; accepted June 30, 2020

Abstract: Various morphologies of magnesium carbonate hydrate had been synthesized without using any organic additives by carefully adjusting the reaction temperature and time during the talc carbonation process. At lower temperatures, magnesium carbonate hydrate was prone to display needle-like morphology. With the further increase of the carbonation temperature, the sheet-like crystallites became the preferred morphology, and at higher aging temperatures, these crystallites tended to assemble into layer-like structures with diverse morphologies, such as rose-like particles and nest-like structure. The reaction time had no effect on the crystal morphology, but it affected the particle size and situation of the crystal growth. X-Ray diffraction results showed that these various morphologies were closely related to their crystal structure and compositions. The needle-like magnesium carbonate hydrate had a formula of $MgCO_3{\cdot}3H_2O$, whereas with the morphological transformation from needle-like to sheet-like, rose-like, and nest-like structure, their corresponding compositions also changed from $MgCO_3{\cdot}3H_2O$ to $4MgCO_3{\cdot}Mg(OH)_2{\cdot}8H_2O$, $4MgCO_3{\cdot}Mg(OH)_2{\cdot}5H_2O$, and $4MgCO_3{\cdot}Mg(OH)_2{\cdot}4H_2O$.

Keywords: magnesium carbonate hydrate, morphology, carbonation temperature, aging temperature

*** Corresponding author: Wenjin Ding,** School of Environment and Resource, Key Laboratory of Ministry of Education for Solid Waste Treatment and Resource Recycle, Southwest University of Science and Technology, Mianyang 621010, China; School of Environment and Resource, Sichuan Engineering Lab of Non-metallic Mineral Powder Modification and High-value Utilization, Southwest University of Science and Technology, Mianyang 621010, China, e-mail: dingwenjin@swust.edu.cn, tel: +86-816-241-9279
Qiuju Chen, Hongjuan Sun, Tongjiang Peng: School of Environment and Resource, Key Laboratory of Ministry of Education for Solid Waste Treatment and Resource Recycle, Southwest University of Science and Technology, Mianyang 621010, China; School of Environment and Resource, Sichuan Engineering Lab of Non-metallic Mineral Powder Modification and High-value Utilization, Southwest University of Science and Technology, Mianyang 621010, China
Tao Hui: School of Environment and Resource, Sichuan Engineering Lab of Non-metallic Mineral Powder Modification and High-value Utilization, Southwest University of Science and Technology, Mianyang 621010, China

1 Introduction

Magnesium carbonate hydrate, as an important magnesia inorganic chemical product, has been widely used in various industrial fields (e.g., filter material, pharmaceuticals, cosmetic manufacturing, rubber industry, lithographing inks, and as precursors for high-purity magnesium oxide [1,2]). Magnesium carbonate hydrate is a class of chemical compounds, and the general formula can be expressed as $xMgCO_3{\cdot}yMg(OH)_2{\cdot}zH_2O$ (x = 1–5, y = 0–1, z = 1–8). Each pair of xyz values corresponds to a material. Each material has its own crystal type and micromorphology. It is generally accepted that the crystal type, micromorphology, and their properties are closely related, and different forms of particles sometimes give different particle properties even for the same substance [3,4]. So, the design and synthesis of magnesium carbonate hydrate with well-controlled morphology are very important.

There have been a large number of chemical methods invented to produce various morphologies of magnesium carbonate hydrate so far. For example, Gautier et al. [5] have studied the growth process of hydromagnesite by calculating its growth kinetics in aqueous solution from 25 to 75°C. Zhang et al. [1] have successfully achieved the magnesium carbonate whiskers by using magnesium salt and sodium bicarbonate solutions, while Guo et al. [6] have found an effective method to adjust the morphology of magnesium carbonate by the reaction of $MgCl_2$ with Na_2CO_3 under the influence of polyacrylamide. Wu et al. [7] have developed a procedure to generate magnesium hydroxide nanoparticles in water-in-oil microemulsions. Wang et al. [8] produced needle-like nesquehonite by the reaction of $MgCl_2$ with $(NH_4)_2CO_3$ in supersaturated solutions. Mitsuhashi et al. [9] have developed a procedure to generate microtube hydromagnesite by the magnesium hydroxide carbonation. Yan and Xue [10] have prepared

Table 1: Conditions of magnesium carbonate hydrate prepared during talc carbonation

No.	Carbonation temperature (°C)	Carbonation time (min)	Aging temperature (°C)	Aging time (h)	Products
1	40	30	60	4	Figure 2a
2	50	30	60	4	Figure 2b
3	60	30	60	4	Figures 1a and 2c
4	80	30	60	4	Figures 1b and 2d
5	40	30	60	4	Figure 3a
6	40	60	60	4	Figure 3b
7	40	90	60	4	Figures 1c and 3c
8	40	120	60	4	Figure 3d
9	40	30	60	4	Figure 4a
10	40	30	70	4	Figure 4b
11	40	30	80	4	Figure 4c
12	40	30	100	4	Figure 4d
13	40	30	100	1	Figure 5a
14	40	30	100	4	Figure 5b
15	40	30	100	8	Figure 5c
16	40	30	100	12	Figures 1d and 5d

nest-like hydromagnesite spheres by a self-assembly of nanosheets in the hydrothermal process. Li et al. [11] have synthesized rose-like hydromagnesite spheres by reacting anhydrous magnesium sulfate and urea via a hydrothermal method. Zhang et al. [3] have found that various morphologies of magnesium carbonate hydrate (including nesquehonite and hydromagnesite) can be synthesized by carefully adjusting the reaction temperature and pH value of the initial reaction solution in a $MgO–CO_2–H_2O$ system during the precipitation process. Through the above analysis, chemical pure substance was the main raw material to produce magnesium carbonate hydrate. To our knowledge, few people have systematically investigated the production of magnesium carbonate hydrate by natural mineral.

Talc is a 2:1 type layered silicate mineral and is abundant in China. Talc shows great physical and chemical properties, which allows us to use it in many fields (e.g., as a filler material, porous material, for the pharmaceutical use, in cosmetics or rubber industry, ceramic [12–18]). This material is also magnesium-rich and can be used as a raw material to prepare magnesium-based chemicals to not only reduce the production cost but also achieve high-value use of talc.

In this study, the magnesium carbonate hydrate with different morphologies was synthesized by talc carbonation without using any organic additives. We systemically investigate the influence of reaction temperature and reaction time on the morphologies of magnesium carbonate hydrate. The preparation method reported herein showed a possibility for high-value utilization of the silicate mineral carbonation product for CO_2 sequestration.

2 Experiment and methods

2.1 Material

Talc powders (SiO_2 62.45; MgO 31.16; Fe_2O_3 0.63; Al_2O_3 0.08; TiO_2 0.1, mass%) were prepared from pristine talc from Guangxi Province, China, by milling with an ignition loss of 5.21. The talc was mingled with some quartz, and talc was the dominating phase. Hydrochloric acid, magnesium chloride, and ammonia were used without further purification. The purity of industry-grade carbon dioxide was 99.9%. The talc powders used in the experiment were ground to less than 15 μm in size.

2.2 Synthesis

The acid-leaching experiment was performed by subjecting talc samples to the hydrochloric acid solution. Approximately 10 g of talc was placed into a 400 mL reaction vessel. A magnetic stir bar was used to ensure adequate mixing throughout the reaction. A hot-bath was utilized to maintain the desired reaction temperature.

The carbonation experiment was performed by subjecting ammonia and carbon dioxide to the acid leaching solution. Magnesium chloride (AR) was added to the acid leaching solution to increase the Mg^{2+} concentration to make it meet the experimental requirement (0.7 mol/L). Industry-grade CO_2 was injected with a predetermined flow rate at normal pressure. A magnetic

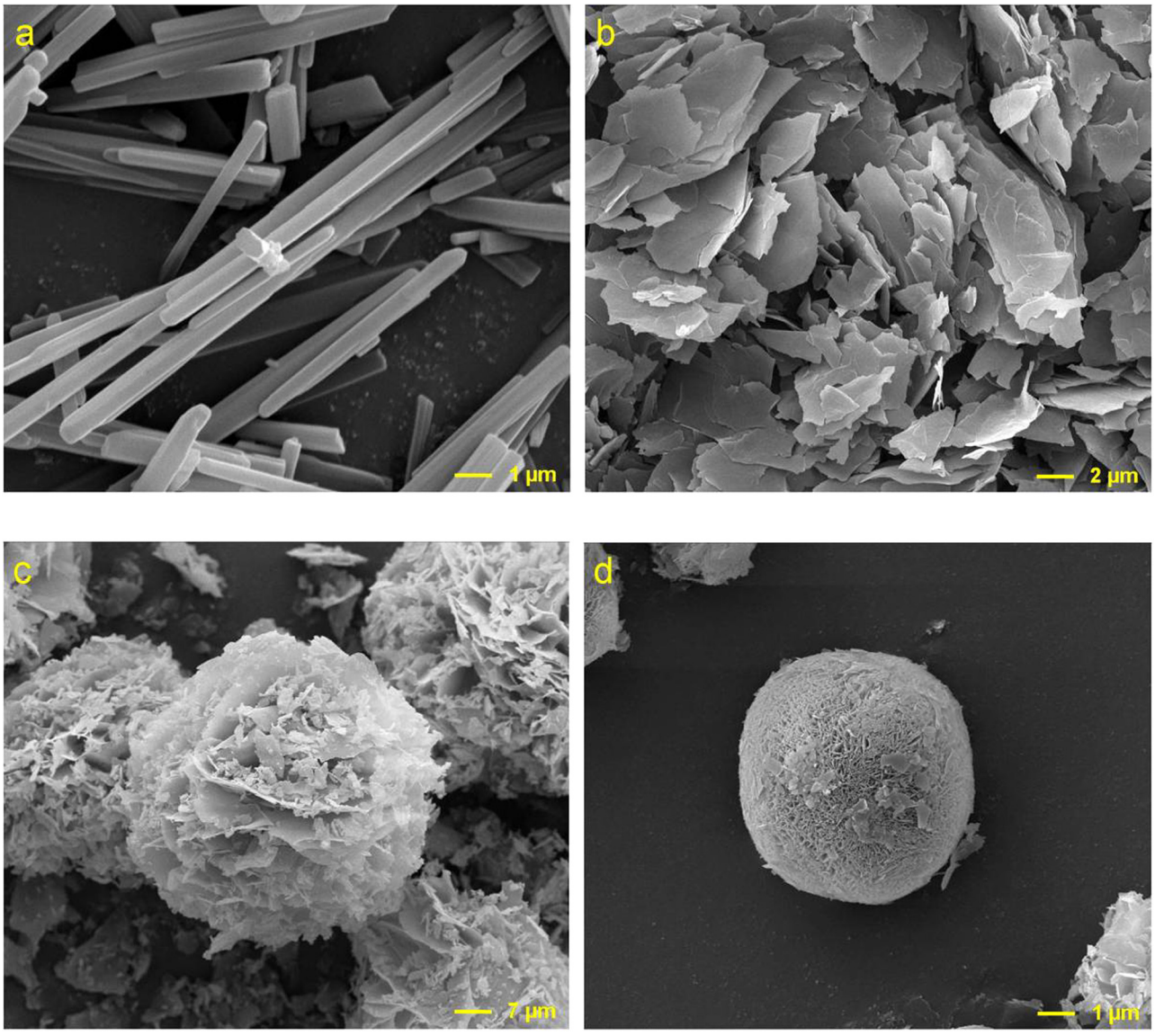

Figure 1: Typical SEM images for the magnesium carbonate hydrate particles during the talc carbonation: (a) needle-like, (b) sheet-like, (c) rose-like, (d) nest-like.

stir bar was used to ensure adequate mixing throughout the reaction. A hot bath was used to maintain the desired reaction temperature. After the desired reaction time, the mixture was aging in a hot bath without stirring at the predetermined temperature and time. Then, the mixture was cooled and filtered to separate the solids from the solution. The solids were then washed with distilled water until they reached a neutral pH, before being dried in an oven at 110°C for 24 h. Detailed experimental conditions for each set of carbonation experiments are listed in Table 1.

2.3 Data analysis

The composition of the sample was determined by X-ray fluorescence and chemical titration. Powder X-ray diffraction (XRD) measurements of the samples were conducted with a DX-2700 X-ray diffractometer using Cu Kα radiation (λ = 0.15406 nm) at a scanning ratio of 0.02 deg/s with a voltage of 40 kV at 40 mA. Scanning electron microscopy (SEM) was performed by a JEOL JSM-6360LV scanning electron microanalyzer with an accelerating voltage of 5 kV.

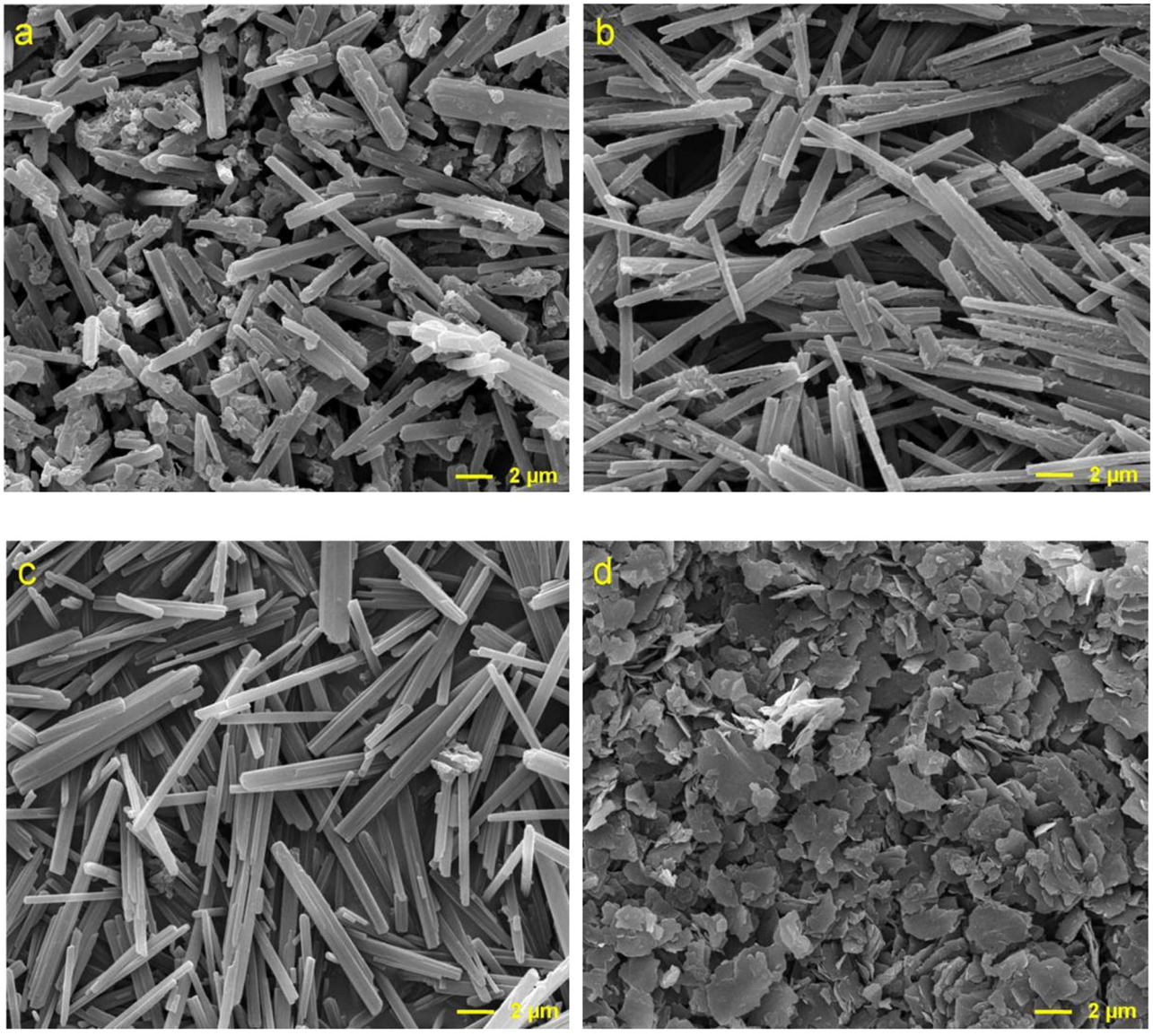

Figure 2: SEM images for the carbonation products with different carbonation temperatures: (a) 40°C, (b) 50°C, (c) 60°C, and (d) 80°C.

Ethical approval: The conducted research is not related to either human or animal use.

3 Results and discussion

3.1 Extraction of magnesium from talc

In a previous study [19], talc-to-enstatite and magnesite-to-periclase transformations were reported when the pristine talc was calcined at 890°C for 60 min. Leaching of magnesium from calcined talc was performed with a 3 mol/L HCl solution at 40°C for 90 min, with a solid-to-liquid ratio of 1:10. Most Mg^{2+} was leached from the thermally activated talc with HCl with a leaching rate up to 95.05%, which benefited the subsequent carbonation reaction.

According to previous experimental results, the reaction temperature and time are known to be important factors for mineral carbonation of magnesium ions. Throughout the carbonation experiment, the concentration of magnesium in the reaction solution, the volume of the reaction solution, the amount of ammonia, and CO_2 flow rate were set to a stoichiometric value that was calculated in our previous study on mineral carbonation for wollastonite [20,21]; these values were 0.7 mol/L, 100 mL, 9 mL, and 200 mL/min, respectively. The following discussion focuses on the impact of reaction temperature and time on the crystal phase and morphology of carbonation products.

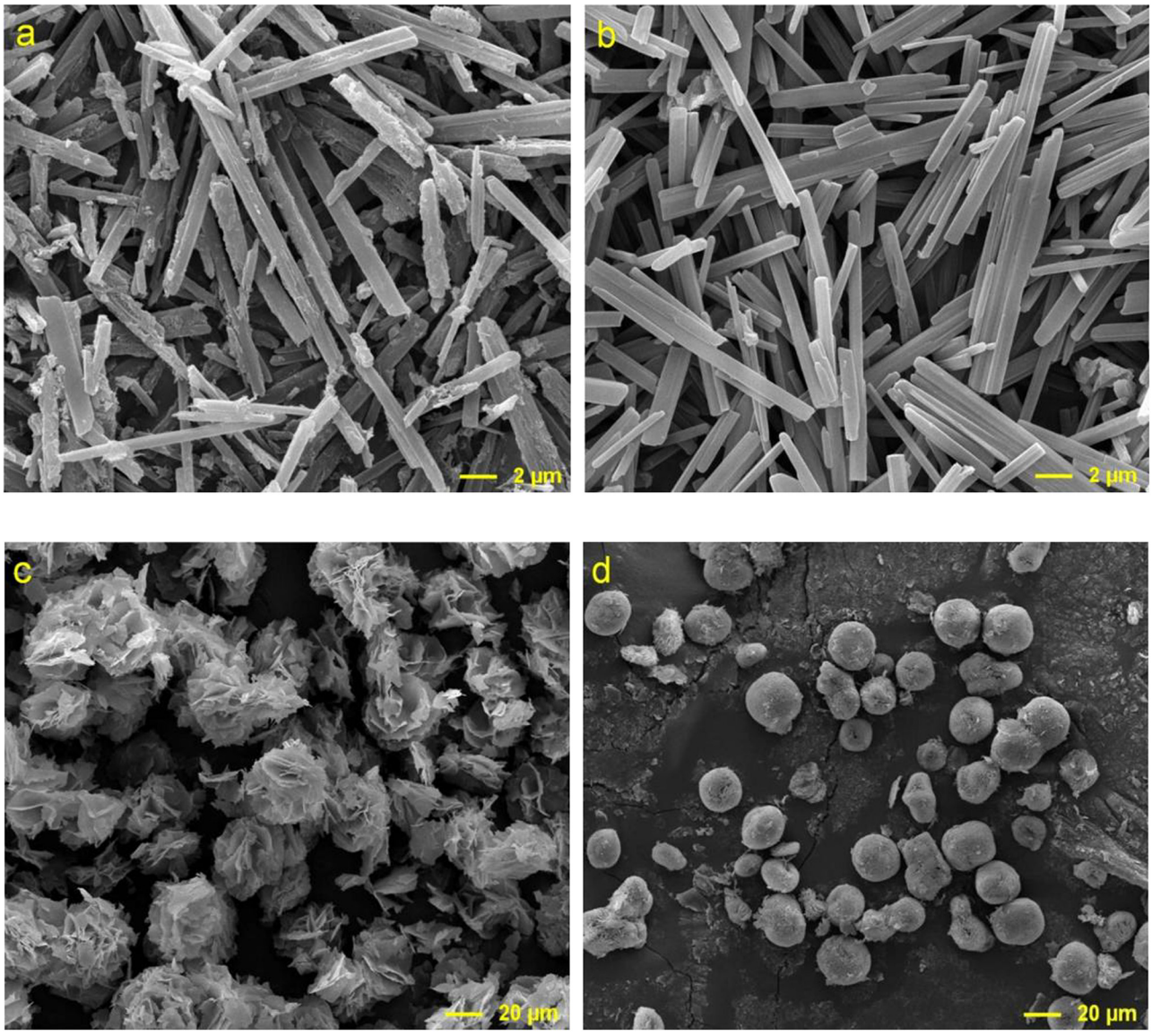

Figure 3: SEM images for the carbonation products with different aging temperatures: (a) 60°C, (b) 70°C, (c) 80°C, and (d) 100°C.

3.2 Production of magnesium carbonate hydrate with different morphologies

The morphology of these magnesium carbonate hydrate particles produced by talc carbonation was visualized by SEM, and the representative images are presented in Figure 1. As can be observed, the magnesium carbonate hydrate particles exhibited four different microscopic morphologies [22–24]. In Figure 1a, the needle-like particles were produced, and the axis diameter was in the range of 0.3–0.8 μm. As can be seen in Figure 1b, the particle displayed sheet-like morphology with a thickness of 40–60 nm. With the further change of reaction parameters, the sheet-like structure would transfer into different layer-like particles, such as rose-like (Figure 1c) and nest-like (Figure 1d) particles.

3.2.1 Effect of reaction temperature

As shown in Figures 2 and 3, these morphologies drastically change with the variation of the reaction temperature. When the carbonation temperature increases from 40 to 60°C, as shown in Figure 2a–c, the needle-like particles were produced, and the average length varies with the increase of the reaction temperature. When the reaction was carried out at 40°C, the length was in the range of 2–8 μm. With the increase of the carbonation temperature,

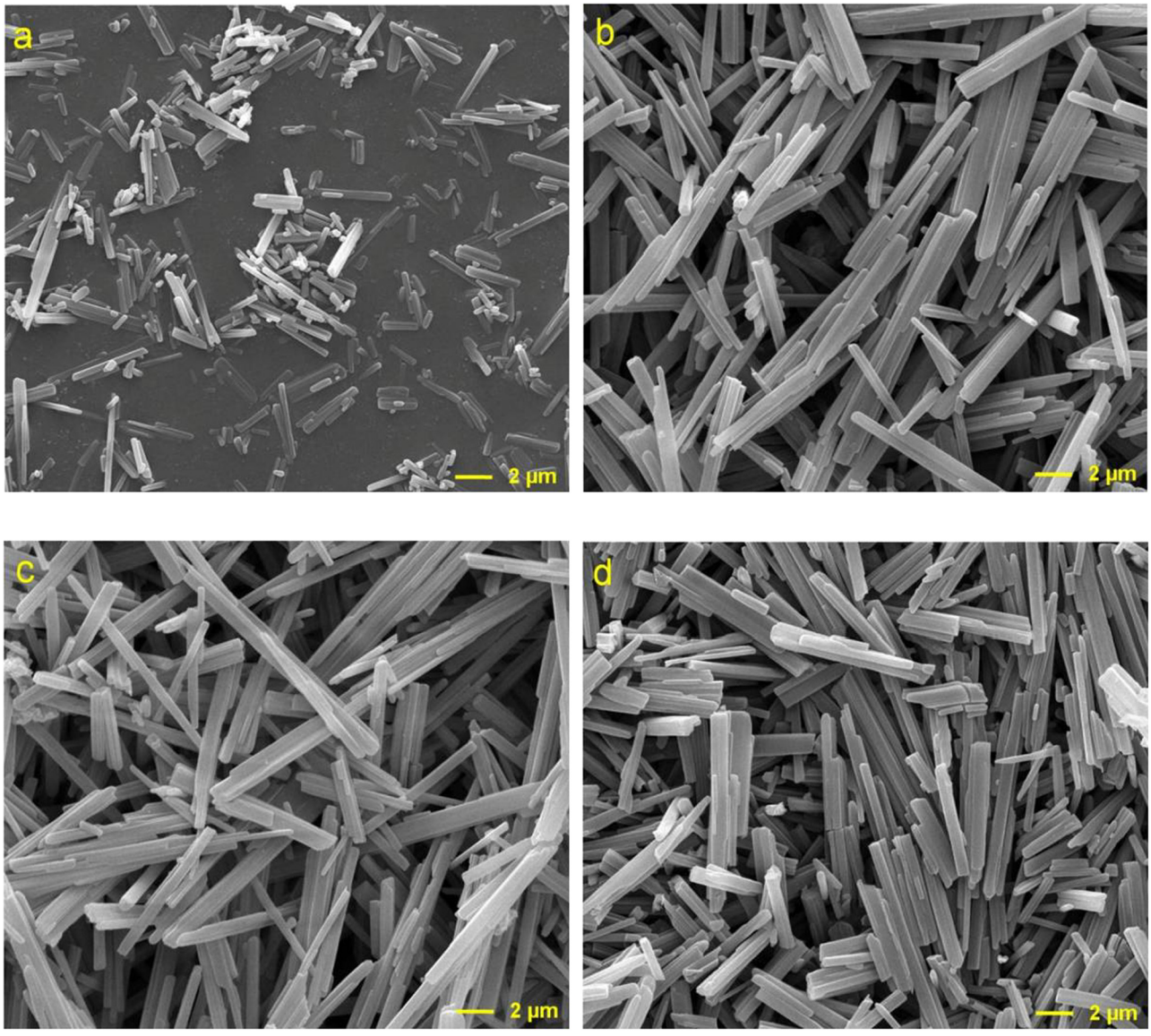

Figure 4: SEM images for the carbonation products from different carbonation times: (a) 30 min, (b) 60 min, (c) 90 min, and (d) 120 min.

the length gradually decreased, and it became 3–14 μm at 50°C. However, further increasing the temperature up to 60°C results in a slight increase of the length, and it became 2–18 μm. This case could be ascribed to the fact that high reaction temperature was more advantageous to the growth of crystals. With the increase of temperature, the viscosity of the initial solution gradually decreased, which accelerated the collision rate of the nuclei. A higher collision rate brought about a higher number of nucleated particles, so it was prone to produce smaller particles. When the temperature reached 60°C, the higher collision rate may also contribute to an increase in the probability of coalescence, and the particle size had a slight increase. This was in line with the predecessors' research results [3]. After careful observation of these needle-like particles in Figure 2a–c, it was clear that the surface structures of these particles became much smoother with the increase of the carbonation temperature. When the carbonation temperature was up to 80°C, a great change in the morphology of the carbonation products took place. As can be seen in Figure 2d, the morphology varied to sheet-like particles with a thickness of 20–40 nm.

The aging temperature also played an important role in the morphology of the carbonation products. When the aging temperatures were 60 and 70°C, all the particles displayed needle-like morphology in Figure 3a and b. As shown in Figure 3c and d when the aging temperature was up to 80°C, the morphology varied from needle-like particles to the rose-like particles [11] with a diameter of 25–40 μm. With the increase of the aging

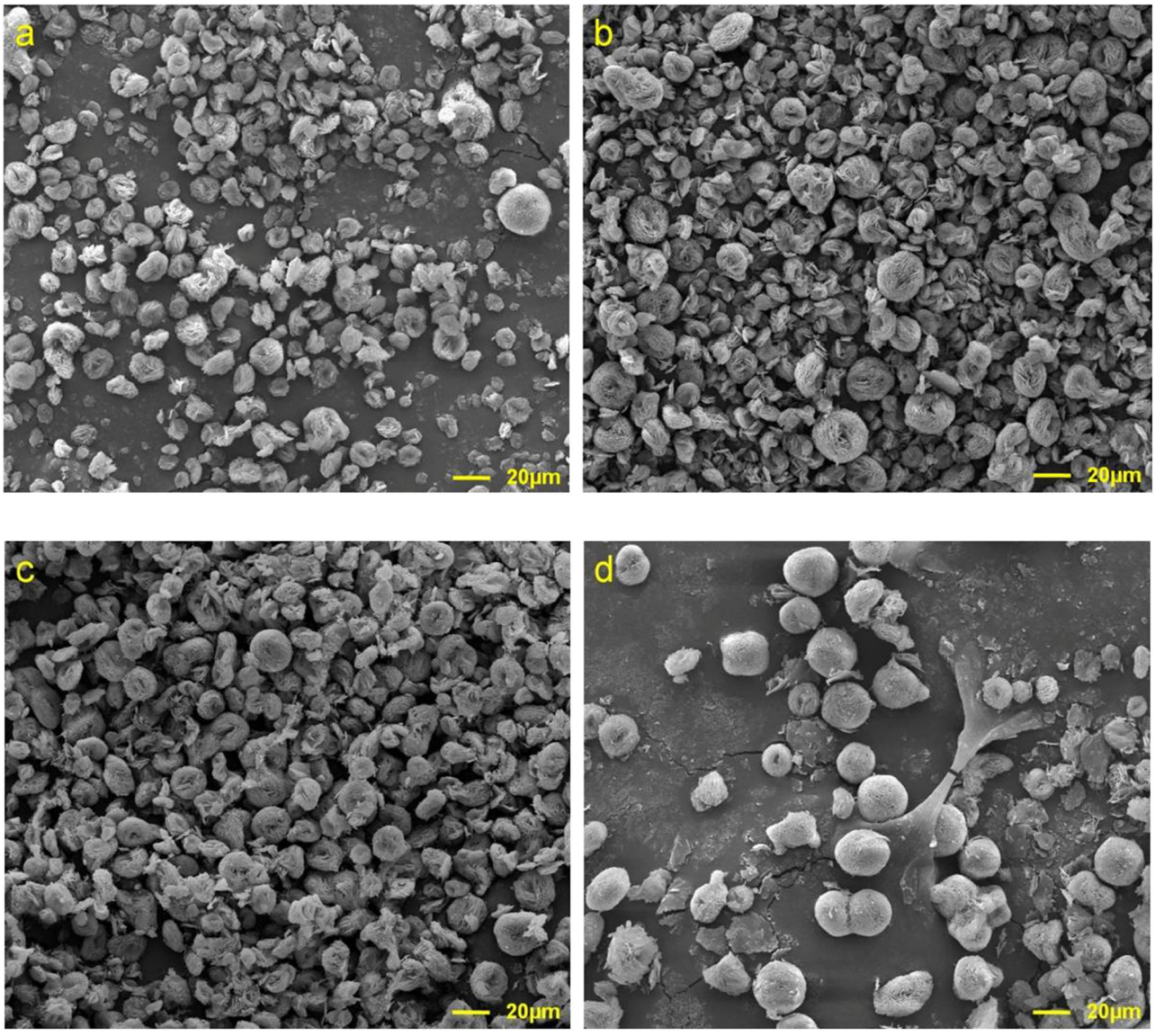

Figure 5: SEM images for the carbonation products from different aging times: (a) 1 h, (b) 4 h, (c) 8 h, and (d) 12 h.

temperature from 80 to 100°C, the particles were prone to display nest-like morphology with a diameter of 15–25 μm [25].

3.2.2 Effect of reaction time

The typical images of the reaction products produced at different carbonation times are shown in Figure 4. At different carbonation times, the particles all displayed a needle-like morphology, but the situation of the crystal growth was different with the extended reaction time, which is obvious in Figure 4a and d. This case could be ascribed to the fact that at a shorter carbonation time (such as 30 min), a small amount of carbon dioxide could dissolve into the solution, and the contact time between Mg^{2+} and CO_3^{2-} was too short. So, the crystal was short and the surface was very coarse. With the increase of the carbonation time, the content of carbon dioxide in the solution increased gradually. It provided sufficient raw materials for the growth of $MgCO_3{\cdot}3H_2O$. As a result, the growth of $MgCO_3{\cdot}3H_2O$ was getting better and better with the further progress of the reaction. At last, the particles formed needle-like morphology with a smooth surface and uniform diameter at the carbonation time of up to 120 min. The morphologies

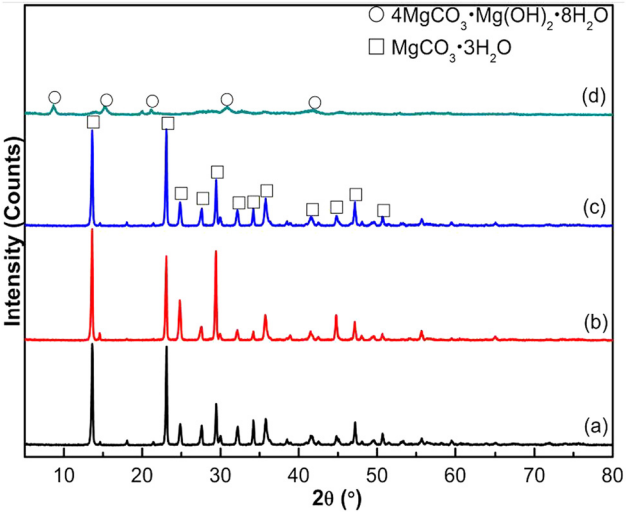

Figure 6: XRD patterns for the carbonation products with different carbonation temperatures: (a) 40°C, (b) 50°C, (c) 60°C, and (d) 80°C.

of the carbonation products produced at different aging times are shown in Figure 5. It had the same conclusion with carbonation time.

3.3 Relationship between the crystal phase and micromorphology of magnesium carbonate hydrate

To better understand the morphology evolution with the variation of temperatures and reaction time, the crystal structure and compositional information of the carbonation product have been recorded by XRD. Figures 6–9 show the corresponding XRD results of these reaction products obtained from different reaction temperatures and time. It was obvious that the XRD patterns varied significantly with the increase of the reaction temperature. For the particles obtained with the carbonation temperature from 40 to 60°C (Figure 6a–c) and the aging temperature from 60 to 70°C (Figure 7a and b), all diffraction peaks in the XRD patterns can be indexed as the monoclinic structure of nesquehonite ($MgCO_3{\cdot}3H_2O$) with unit cell parameters of a = 12.11, b = 5.37, and c = 7.70 Å and $\alpha = \gamma = \beta = 90°$, which are in good agreement with the reported data (JCPDS Card 020-0669). Research about crystal structure suggests that $MgCO_3{\cdot}3H_2O$ formed a 1D chain-like structure by [MgO_6] octahedral. Along the direction of the lattice plane (010), [MgO_6] octahedral is closely linked by Mg–O. So, the growth of the lattice plane (010) is the fastest, and $MgCO_3{\cdot}3H_2O$ is prone to form chain-like structure along the direction and to display needle-like morphology [26]. With the increase of the carbonation temperature up to 80°C (Figure 6d), the XRD pattern underwent a great change. Nesquehonite was transformed into dypingite ($4MgCO_3{\cdot}Mg(OH)_2{\cdot}8H_2O$, JCPDS Card 029-0857). Research about crystal structure suggests that the growth of $4MgCO_3{\cdot}Mg(OH)_2{\cdot}8H_2O$ along (100) and (001) face is faster, and the crystal is prone to form 2D structure and to display sheet-like morphology. When the aging temperature was up to 80–100°C, the crystal phase of the reaction products was transformed into dypingite ($4MgCO_3{\cdot}Mg(OH)_2{\cdot}5H_2O$, JCPDS Card 023-1218) and hydromagnesite ($4MgCO_3{\cdot}Mg(OH)_2{\cdot}4H_2O$, JCPDS Card 025-0513), respectively (Figure 7c and d). Figure 8 provides a set of XRD patterns corresponding to the samples from different carbonation times. As can be observed, the only crystal phase was nesquehonite at different carbonation times. The intensity of the crystal diffraction peaks was gradually increased with an increase of the carbonation time, well consistent with the SEM results. The XRD results of the reaction products produced at different aging times are shown in Figure 9. The only crystal phase was hydromagnesite at different aging times. And the intensity of the crystal diffraction peaks was gradually increased with an increase of the aging time. These results suggested that the reaction products exhibit four different microscopic morphologies. The reaction products of the crystal phase for nesquehonite ($MgCO_3{\cdot}3H_2O$) displayed needle-like morphology, and the products of the crystal phase for dypingite ($4MgCO_3{\cdot}Mg(OH)_2{\cdot}8H_2O$) displayed sheet-like morphology. The reaction products of the sheet-like structure would transfer into different layer-like particles,

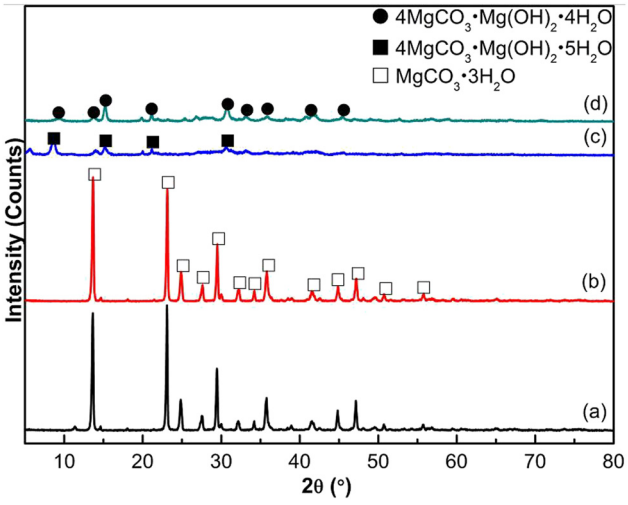

Figure 7: XRD patterns for the carbonation products with different aging temperatures: (a) 60°C, (b) 70°C, (c) 80°C, and (d) 100°C.

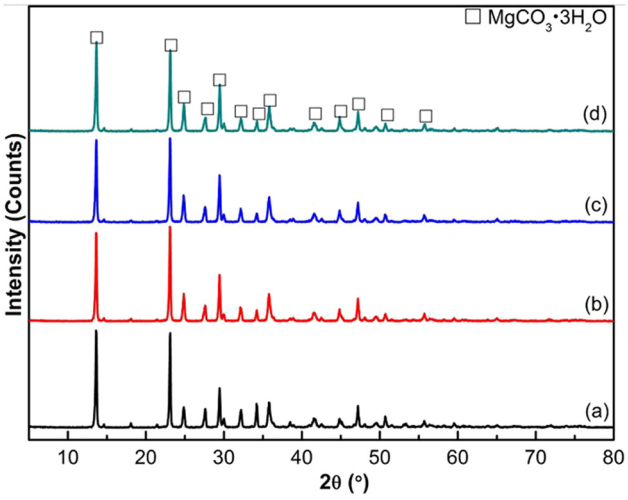

Figure 8: XRD patterns for the carbonation products from different carbonation times: (a) 30 min, (b) 60 min, (c) 90 min and (d) 120 min.

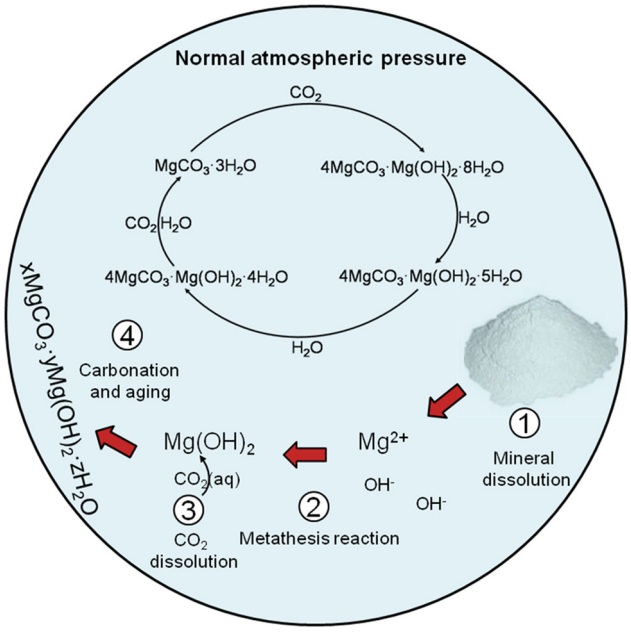

Figure 10: Schematic diagram of the production of magnesium carbonate hydrate with different morphologies during talc carbonation.

such as rose-like and nest-like particles. The assembly process had something to do with the reaction temperature (including carbonation temperature and aging temperature).

3.4 Production mechanism

The aqueous production reaction in the gas–liquid–solid system is irreversible and heterogeneous due to the low porosity of the materials. The proposed production processes are shown in equations (1)–(6). First, ammonia reacts with magnesium chloride to form magnesium hydroxide [27], which then forms magnesium bicarbonate through reaction with carbon dioxide. Magnesium bicarbonate then forms into nesquehonite in solution with aging. Nesquehonite converted to dypingite ($4MgCO_3{\cdot}Mg(OH)_2{\cdot}8H_2O$, $4MgCO_3{\cdot}Mg(OH)_2{\cdot}5H_2O$) and hydromagnesite with different aging temperatures.

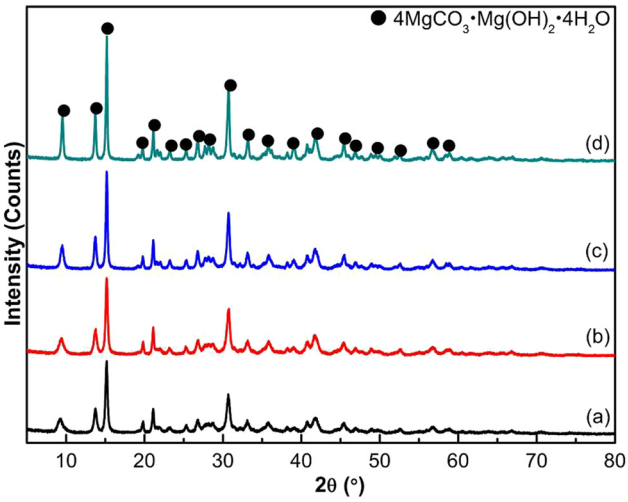

Figure 9: XRD patterns for the carbonation products from different aging times: (a) 1 h, (b) 4 h, (c) 8 h, and (d) 12 h.

$$MgCl_2 + 2NH_3{\cdot}H_2O \rightarrow Mg(OH)_2 \downarrow + 2NH_4Cl \quad (1)$$

$$Mg(OH)_2 + 2CO_2 \xrightarrow{\text{carbonize}} Mg(HCO_3)_2 \quad (2)$$

$$Mg(HCO_3)_2 + 2H_2O \xrightarrow{\text{aging}} MgCO_3{\cdot}3H_2O + CO_2 \quad (3)$$

$$5MgCO_3{\cdot}3H_2O + 6H_2O \xrightarrow{\text{aging}} 4MgCO_3{\cdot}Mg(OH)_2{\cdot}8H_2O + CO_2 \quad (4)$$

$$4MgCO_3{\cdot}Mg(OH)_2{\cdot}8H_2O \xrightarrow{\text{aging}} 4MgCO_3{\cdot}Mg(OH)_2{\cdot}5H_2O + 3H_2O \quad (5)$$

$$4MgCO_3{\cdot}Mg(OH)_2{\cdot}5H_2O \xrightarrow{\text{aging}} 4MgCO_3{\cdot}Mg(OH)_2{\cdot}4H_2O + H_2O. \quad (6)$$

During carbonation with gypsum desulfurization [28], ammonia was used to generate ammonium bicarbonate (or carbonate). The two systems have different reaction mechanisms. Based on the above analysis, the following three-step mechanism of talc carbonation can be summarized: (a) Mg^{2+} is leached from pristine talc, (b) magnesium chloride is transformed into magnesium

hydroxide via reaction with ammonia, and (c) to magnesium carbonate hydrate with different polymorph and morphology forms via reaction with CO_2 (g) injected in the solution and magnesium hydroxide (Figure 10).

4 Conclusions

We demonstrated a facile route for the production of magnesium carbonate hydrate with talc as a raw material. Main productions and results were as follows: (1) magnesium carbonate hydrate can display four different morphologies during the reaction process, (2) at reaction temperatures (including carbonation temperature and aging temperature) below 80°C, the magnesium carbonate hydrate particles were all prone to assemble into needle-like morphology, which had a formula of $MgCO_3{\cdot}3H_2O$, the size and growth situation of the needle-like particle can be adjusted by the reaction time, (3) at reaction temperatures (including carbonation temperature and aging temperature) above 80°C, the sheet-like structure was the preferred morphology, and it had a formula of $4MgCO_3{\cdot}Mg(OH)_2{\cdot}8H_2O$; with an further increase of reaction temperature, the sheet-like structure would transfer into different layer-like particles, such as rose-like and nest-like particles. The method of the synthesis of magnesium carbonate hydrate described here may serve a promising basis for systemically studying the application of the mineral carbonation product for CO_2 sequestration.

Acknowledgments: This work was supported by the doctoral foundation of Southwest University of Science and Technology (17zx7117), the Longshan academic talent research, and the Innovation Team Project of SWUST (18lzx401).

Conflict of interest: The authors declare no conflict of interest.

References

[1] Zhang H, Chang Z, Qian X, An X. *In situ* preparation, characterization and performance of magnesium carbonate whiskers/cellulose fibers hybrid paper. Cellulose. 2014;21(6):4633–41.

[2] Zajac M, Durdzinski P, Stabler C, Skocek J, Nied D, Ben Haha M. Influence of calcium and magnesium carbonates on hydration kinetics, hydrate assemblage and microstructural development of metakaolin containing composite cements. Cement Concrete Res. 2018;106:91–102.

[3] Zhang Z, Zheng Y, Ni Y, Liu Z, Chen J, Liang X. Temperature- and pH-dependent morphology and FT-IR analysis of magnesium carbonate hydrates. J Phys Chem B. 2006;110(26):12969–73.

[4] Wang D, Xu L, Nai J, Bai X, Sun T. Morphology-controllable synthesis of nanocarbons and their application in advanced symmetric supercapacitor in ionic liquid electrolyte. Appl Surf Sci. 2019;473:1014–23.

[5] Gautier Q, Bénézeth P, Mavromatis V, Schott J. Hydromagnesite solubility product and growth kinetics in aqueous solution from 25 to 75°C. Geochim Cosmochim Acta. 2014;138:1–20.

[6] Guo M, Li Q, Ye X, Wu Z. Magnesium carbonate precipitation under the influence of polyacrylamide. Powder Technol. 2010;200(1–2):46–51.

[7] Wu J, Yan H, Zhang X, Wei L, Liu X, Xu B. Magnesium hydroxide nanoparticles synthesized in water-in-oil microemulsions. J Colloid Interface Sci. 2008;324(1–2):167–71.

[8] Wang Y, Li Z, Demopoulos GP. Controlled precipitation of nesquehonite ($MgCO_3{\cdot}3H_2O$) by the reaction of $MgCl_2$ with $(NH_4)_2CO_3$. J Cryst Growth. 2008;310(6):1220–7.

[9] Mitsuhashi K, Tagami N, Tanabe K, Ohkubo T, Sakai H, Koishi M, et al. Synthesis of microtubes with a surface of "house of cards" structure via needlelike particles and control of their pore size. Langmuir. 2005;21(8):3659–63.

[10] Yan C, Xue D. Novel self-assembled MgO nanosheet and its precursors. J Phys Chem B. 2005;109(25):12358–61.

[11] Li Q, Ding Y, Yu GH, Li C, Li FQ, Qian YT. Fabrication of light-emitting porous hydromagnesite with rosette-like architecture. Solid State Commun. 2003;125(2):117–20.

[12] Tábi T, Suplicz A, Czigány T, Kovacs JG. Thermal and mechanical analysis of injection moulded poly(lactic acid) filled with poly (ethylene glycol) and talc. J Therm Anal Calorim. 2014;118(3):1419–30.

[13] Rane RH, Jayaraman K, Nichols KL, Bieler TR, Mazor MH. Evolution of crystalline orientation and texture during solid phase die-drawing of PP-talc composites. J Polym Sci Part B Polym Phys. 2014;52(23):1528–38.

[14] Li G, Tavangarian F. Sintering behavior, microstructure and mechanical properties of vacuum sintered SiC/spinel nanocomposite. J Alloys Compd. 2014;615:204–10.

[15] Yu W, Wang X, Ferraris E, Zhang J. Melt crystallization of PLA/Talc in fused filament fabrication. Mater Des. 2019; 182:1–6.

[16] Llewelyn G, Rees A, Griffiths CA, Jacobi M. A novel hybrid foaming method for low-pressure microcellular foam production of unfilled and talc-filled copolymer polypropylenes. Polymers. 2019;11(11):1–15.

[17] Lima LCB, Coelho CC, Silva FC, Meneguin AB, Barud HS, Bezerra RDS, et al. Hybrid systems based on talc and chitosan for controlled drug release. Materials. 2019;12(21):1–17.

[18] Ghanbari A, Behzadfar E, Arjmand M. Properties of talc filled reactor-made thermoplastic polyolefin composites. J Polym Res. 2019;26(10):1–8.

[19] Ding W, Ouyang J, Yang H. Synthesis and characterization of nesquehonite (MgCO3·3H2O) powders from natural talc. Powder Technol. 2016;292:169–75.

[20] Ding W, Yang H, Ouyang J, Long H. Modified wollastonite sequestrating CO2 and exploratory application of the carbonation products. RSC Adv. 2016;6(81):78090–9.
[21] Ding W, Fu L, Ouyang J, Yang H. CO_2 mineral sequestration by wollastonite carbonation. Phys Chem Min. 2014;41(7):489–96.
[22] Montes-Hernandez G, Renard F, Chiriac R, Findling N, Toche F. Rapid precipitation of magnesite microcrystals from Mg $(OH)_2$–H_2O–CO_2 slurry enhanced by NaOH and a heat-aging step (from ~20 to 90°C). Cryst Growth Des. 2012;12(11):5233–40.
[23] Harrison AL, Mavromatis V, Oelkers EH, Benezeth P. Solubility of the hydrated Mg-carbonates nesquehonite and dypingite from 5 to 35 degrees C: implications for CO_2 storage and the relative stability of Mg-carbonates. Chem Geol. 2019;504:123–35.
[24] Oelkers EH, Berninger U-N, Perez-Fernandez A, Chmeleff J, Mavromatis V. The temporal evolution of magnesium isotope fractionation during hydromagnesite dissolution, precipitation, and at equilibrium. Geochim Cosmochim Acta. 2018;226:36–49.
[25] Zhang ZP, Zheng YJ, Zhang JX, Zhang Q, Chen JP, Liu ZM, et al. Synthesis and shape evolution of monodisperse basic magnesium carbonate microspheres. Cryst Growth Des. 2007;7(2):337–42.
[26] Giester G, Lengauer CL, Rieck B. The crystal structure of nesquehonite, $MgCO_3{\cdot}3H_2O$, from Lavrion, Greece. Min Petrol. 2000;70(3–4):153–63.
[27] Ding W, Chen Q, Sun H, Peng T. Modified phosphogypsum sequestrating CO_2 and characteristics of the carbonation product. Energy. 2019;182:224–35.
[28] Ding W, Yang H, Ouyang J. Mineral carbonation of a desulfurization residue for CO_2 sequestration. RSC Adv. 2015;5(82):67184–94.